Simulations of the Strong–Strong Beam–Beam Interaction in Hadron Colliders

J. A. Ellison, M. Vogt, UNM, Albuquerque, NM 87131, USA
T. Sen, FNAL, Batavia, IL 60510, USA

Abstract

We develop weighted macro–particle tracking and the Perron–Frobenius operator technique for simulating the time evolution of two beams coupled via the beam–beam interaction. The π- and σ–modes, with and without a sextupole perturbation, are studied based on the Vlasov-Poisson system. Extending standard averaging formalism to maps with a small collective force, we derive an approximation to the "kick-rotate" model of our simulation. This eliminates the delta function smoothing in the Vlasov equation, common in many theoretical approaches. Action densities are quasi-equilibria, consistent with simulation, and linearization leads to uncoupled Fourier modes and third–kind integral equations. Extensions to 2–d.o.f. and a flexible general purpose code are being developed.

1 MODEL AND ANALYSIS

1.1 The Kick-Rotate Model

Let $\psi_n(x)$ and $\psi_n^*(x)$, $x = (q,p)^{\mathrm{T}}$, denote the phase space densities of the two counter-rotating beams just before the IP at turn n. Then the evolution of a particle in the unstarred beam is given by

$$x_{n+1} = R[x_n + \xi\,(0,1)^{\mathrm{T}}(G * \psi_n^*)(x_n)] \quad . \qquad (1)$$

Here R is rotation thru an angle $\mu = 2\pi Q$ ($\alpha = 0$ and $\beta = 1$) and $(G*\psi)(x) := \int_{\mathbb{R}^2} G(q-q')\psi(x')dx'$, for response function G. The evolution law for the starred beam is given by (1) with ψ_n^* replaced by ψ_n. The transformation (1) is symplectic so $\psi_{n+1}(x_{n+1}) = \psi_n(x_n)$. Defining "angle"-action variables, $x_n =: \sqrt{2J_n}(\cos\alpha_n, -\sin\alpha_n)^{\mathrm{T}}$, where $\alpha_n = n\mu - \Theta_n$, the evolution law becomes

$$\begin{aligned}\Theta_{n+1} &= \Theta_n + \xi A\frac{1}{\sqrt{2J_n}}\cos\alpha_n + O(\xi^2)\\ J_{n+1} &= J_n - \xi A\sqrt{2J_n}\sin\alpha_n + O(\xi^2) \quad , \qquad (2)\end{aligned}$$

where $A(n\mu, \Theta_n, J_n, ; \Psi_n^*) = \int_{\mathcal{C}} G\Psi_n^* d\Theta' dJ'$ and $\mathcal{C} := [0,2\pi) \times [0,\infty]$. Here $G = G(\sqrt{2J_n}\cos(n\mu - \Theta_n) - \sqrt{2J'}\cos(n\mu - \Theta'))$ and $\Psi_n^*(\Theta, J) = \psi_n^*(\sqrt{2J}\cos(n\mu - \Theta), -\sqrt{2J}\sin(n\mu - \Theta))$.

1.2 Map–Averaging

Equations (2) are in a standard form for averaging as (Θ_n, J_n) and Ψ_n^* are slowly varying for small ξ. The averaged equations are obtained by dropping the $O(\xi^2)$ term and averaging the rhs over n holding the slowly varying quantities fixed. We write $\Theta_{n+1} = \Theta_n + \xi k_1(\Theta_n, J_n; \Psi_n^*)$ and $J_{n+1} = J_n - \xi k_2(\Theta_n, J_n; \Psi_n^*)$. Inverting these through $O(\xi)$ gives the averaged evolution law for the densities:

$$\Psi_{n+1}(\Theta, J) = \Psi_n(\Theta - \xi k_1(\Theta, J; \Psi_n^*), J + \xi k_2(\Theta, J; \Psi_n^*)) \qquad (3)$$

and a similar equation for the starred beam. Equation (3), with the corresponding equation for the starred beam, is our basic model. In the CR model [1] $G(q) = \mathrm{sgn}(q)$ where sgn is the signum function. The Birkhoff ergodic theorem gives the average of $\sin(n\mu - \theta)\mathrm{sgn}(\cos(n\mu - \theta))$ equals the $t-$average of $\sin(t)\mathrm{sgn}(\cos(t))$ which is zero and $2/\pi$ if $\sin$ is replaced by $\cos$, for almost all θ if $\mu/2\pi$ is irrational. Thus $k_j(\Theta, J; \Psi) = \int_{\mathcal{C}} K_j(J, J', \Theta - \Theta')\Psi(\Theta', J')d\Theta' dJ'$ where $K_1 = (2/\pi)\partial_J D$ and $K_2 = (2/\pi)\partial_\Theta D$ for $D = \sqrt{2J + 2J' - 4\sqrt{JJ'}\cos\Theta}$.

If Ψ_0 and Ψ_0^* depend only on J then $\Psi_n(\Theta, J) = \Psi_0(J)$ and $\Psi_n^*(\Theta, J) = \Psi_0^*(J)$. This follows from the fact that $k_2(\Theta, J; \Psi(J)) = 0$ since K_2 is an odd function of Θ. Thus functions only of J are equilibria for the averaged model and thus quasi-equilibria for (1).

Fig. 1 shows the action density for about 100 n in the interval from 0 to 2^{17} for two cases based on a PF simulation. In the first case (red crosses) the initial density is a function of the action alone and to the eye there is no change. In the second case (green X-es) the offset of both beams ($\pm 1\sigma_0$) leads to a Θ dependence and we see the action density evolves. Thus $\xi = 0.003$ is within the averaging approximation on this time interval.

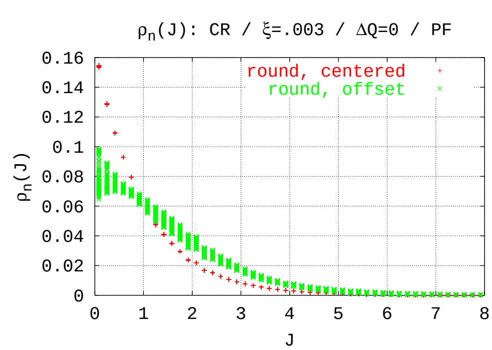

Figure 1: The action density

1.3 *The Linearized Equations*

Here we study the behavior of solutions of (3) in an ϵ-neighborhood of an equilibrium, thus we write $\Psi_n(\Theta, J) = \Psi_e(J) + \epsilon F_n(\Theta, J)$ and the corresponding equation for the starred beam. Plugging into (3) and dropping higher order terms yields $F_{n+1} - F_n = \xi[\Psi_e'(J) k_2(\Theta, J; F_n^*) - \partial_\Theta F_n(\Theta, J) k_1(\Theta, J; \Psi_e)]$. Clearly, $\omega(J) := k_1(\Theta, J; \Psi_e)$ is independent of Θ and is the tune shift in the weak-strong case where the strong beam has density Ψ_e. Defining $H := F \pm F^*$, we obtain our basic integro-difference equations:

$$H_{n+1}(\Theta, J) - H_n(\Theta, J) = -\xi\omega(J)\partial_\Theta H_n(\Theta, J) \pm \xi\Psi_e'(J)\int_C K(J, J', \Theta - \Theta')H_n(\Theta', J')d\Theta' dJ' \quad , \quad (4)$$

for the σ and π equations respectively.

Because of the convolution structure of (4), the Fourier coefficients $h_{n,k}(J)$ of $H_n(\cdot, J)$ are uncoupled and evolve by $h_{n+1,k}(J) - h_{n,k}(J) = \xi[\pm ik\omega(J)h_{n,k}(J) + \Psi_e'(J)\int_0^\infty K_k(J, J')h_{n,k}(J')dJ']$, where $K_k/2\pi$ is the kth Fourier coefficient of $K(J, J', \cdot)$. To analyze the stability, we note that the equation for the Fourier modes is equivalent to $\partial_t h(J,t) = \xi[\pm ik\omega(J)h(J,t) + \Psi_e'(J)\int_0^\infty K_k(J,J')h(J',t)dJ'] + O(\xi^2)$. Taking the Laplace transform gives

$$[s \mp ik\xi\omega(J)]\tilde{h}(J,s) = \xi\Psi_e'(J)\int_0^\infty K_k(J, J')\tilde{h}(J', s)dJ' + h(J, 0) \quad . \quad (5)$$

Equation (5) is a nonhomogeneous integral equation of the third kind. An identical homogeneous equation is obtained from the ansatz $h_{n,k}(J) = a^n\phi_k(J, a)$. We are presently analyzing these equations and are in the process of developing a weakly nonlinear theory to see coupling of Fourier modes.

2 SIMULATIONS

The Perron–Frobenius (PF) and weighted macro–particle tracking (WMPT) methods have been developed. Both are based on the evolution law $\psi_{n+1}(x) = \psi_n(T^{-1}(x; \psi_n^*))$ given a symplectic one turn map (OTM) T as in (1).

The PF method [2] directly applies this evolution law on a square grid $\{x_{ij}\}$, $1 \le i,j \le n_g$. An approximation $\tilde{\psi}_{ij}(n)$ to the density $\psi_n(x_{ij})$ is obtained by tracking x_{ij} backward to $T^{-1}(x_{ij}; \psi_n^*)$ and interpolating the density between its neighboring grid points. WMPT [3] is a method for computing time dependent phase space averages of f via $\langle f\rangle_n := \int_{\mathbb{R}^2} f(x)\psi_n(x)\, d^2x = \int_{\mathbb{R}^2} f(M_n(x))\psi_0(x)\, d^2x$, where M_n is the symplectic n–turn map containing the collective force. Averages are approximated by

$$\langle f\rangle_n \approx \begin{cases} \sum_{ij} f(x_{ij})\tilde{\psi}_{ij}(n)w_{ij} & : \text{PF} \\ \sum_{ij} f(M_n(x_{ij}))\psi_{ij}(0)w_{ij} & : \text{WMPT} \end{cases} \quad . \quad (6)$$

where w_{ij} are quadrature weights. Note that $(G * \psi_n^*)(q) = \langle G(\cdot, q)\rangle_n^*$, but generally its numerical evaluation for off–grid trajectories has an operations count of $O(n_g^{4d})$ in d d.o.f. We study the centroids $\bar{q}_n^{\sigma,\pi} := \langle q\rangle_n \pm \langle q\rangle_n^*$, as well as the beam emittance.

2.1 *Some Results in one d.o.f.*

The beam–beam interaction is a 2–d.o.f. process. However as a starting point for WMPT we have compared three different 1–d.o.f. limiting cases [3], a flat beam and motion in the vertical phase plane (CR) [1], a round beam (AS) [3], and a flat beam and motion in the horizontal phase plane (YO) [4]. For CR we found a completely selfconsistent WMPT representation of the collective force with an operations count of only $O(N \log N)$, $N = n_g^4$. For AS & YO the operation count for a completely selfconsistent WMPT evolution is $O(N^2)$. Thus, we simulated them by approximating the starred density in (1) by a Gaussian with the moments calculated from the starred beam so that the collective force can be evaluated analytically. This approximation (GSA) is often used, [3, 5]. The tune difference of the modes obtained by FFT from the time discrete data of $\bar{q}_n^\sigma$ and $\bar{q}_n^\pi$ as well as the separation of the unperturbed (linear) tunes needed to establish phase mixing (damping) depends on the limiting case [3].

Fig. 2 shows good agreement between the spectra of the σ- and π–mode obtained with PF and WMPT for $\xi = 0.003$ and almost identical linear tunes $Q_0 = \sqrt{5} - 2$ in the CR limit, giving confidence in the methods. Both beams were initially standard Gaussians with the unstarred beam offset by $0.1\sigma_0$. The initial density was represented by a 201×201 square grid over $\pm 5\sigma_0$ in both directions for WMPT and the grid for the PF simulation used 241×241 points over $\pm 6\sigma_0$. The FFT was performed over data from 2^{17} turns. The two σ–mode spectra (peak on right) are almost indistinguishable. The two π–mode spectra have nearly the same tune and the continuum due to the single particle motion is quite pronounced in the WMPT spectrum.

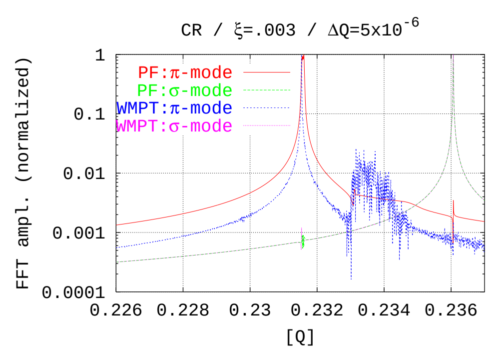

Figure 2: Comparison between PF and WMPT

Fig. 3 shows the emittance growth induced by the interaction of a strong sextupole kick in the center of the arc and a strong beam–beam interaction in the CR limit close to the third–integer resonance. Both beams were initially round and one had a $0.1\sigma_0$ offset. The sextupole alone (blue curve) (or with ξ up to .006) leads to hardly any emittance growth. However, when the incoherent tune spread reaches $1/3$ ($\xi = .009$, green) the emittance is significantly increased. Moreover, in the latter case the π–mode amplitude is enhanced from about $0.1\sigma_0$ to about $1.5\sigma_0$ whereas the σ–mode amplitude stays small (both not shown). Finally when the $1/3$ resonance is well inside the incoherent tune spread ($\xi = 0.012$, red), the emittance grows strongly and the amplitudes of both modes are significantly enhanced (not shown).

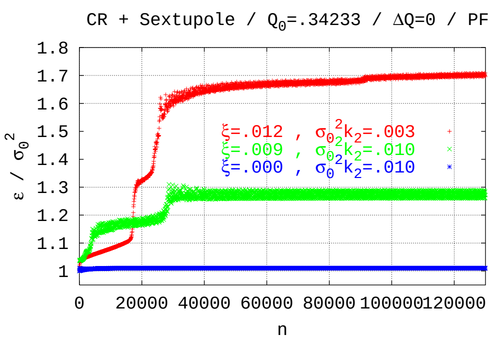

Figure 3: Emittance growth with beam–beam and Sextupole. PF with 401×401 over $\pm6\sigma_0$. $\sigma_0^2 k_2$ is the normalized sextupole strength.

2.2 *Preliminary results in two d.o.f.*

We are modifying the PF and WMPT codes to work in the 4–D transverse phase space (BBPF2D, BBDeMo2D). Initial results for PF show that with a 51^4 grid and 4-D cubic interpolation the probability is not satisfactorily conserved even for a short time. We hope to improve the 4–D PF performance by higher order local or global (spline) interpolation. WMPT conserves probability by construction, however it requires attention in order to avoid an operations count per turn of $O(n_g^8)$. So far we have implemented two approaches into BBDeMo2D. The GSA approach which is clearly $O(n_g^4)$ [5] and the Hybrid Fast Multipole Method (HFMM) [6] which is also approximately $O(n_g^4)$. However, the simulations in 4–D phase space require enormous amount of (real) memory and computation time and we are pursuing parallel versions.

Fig. 4 shows preliminary results for the spectra of the π_x- and σ_x–modes for initially round Gaussian beams with WMPT over 2^{13} turns. The GSA used 51^4 particles and the selfconsistent HFMM used 45^4 particles, both over a $\pm5\sigma_0$ initial grid. The π_x- and σ_x–modes can clearly be resolved. Note that the two σ_x–mode spectra in this resolution are almost on top of one another. The modes in the y–plane (not shown) behave the same. The ratio $\varepsilon_{x,n}/\varepsilon_{y,n}$ stays very close to $1 \equiv \varepsilon_{x,0}/\varepsilon_{y,0}$. The deviation from one is less than 10% which is well below the expected resolution of these runs. The separation of the π_x–mode tune from the σ_x–mode tune is $(1.4\pm0.1)\xi_x$ in the GSA and $(1.5\pm0.1)\xi_x$ with HFMM. The single particle continuum, visible in the π–mode spectra, is a little more pronounced with HFMM.

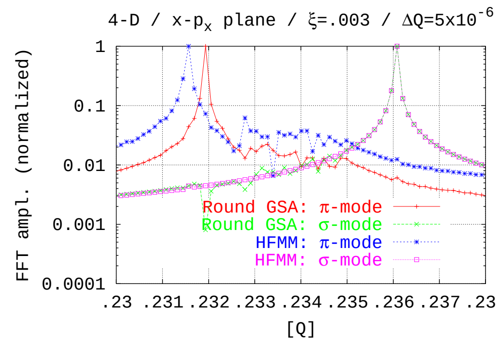

Figure 4: The spectra of the π_x- and σ_x–mode computed with BBDeMo2D with 51^4 particles in the round GSA (red, green) and with 45^4 particles in the HFMM approach (blue, purple).

3 OUTLOOK

WMPT and PF show good agreement in the 1 d.o.f cases thus we are extending both to the more important 2 d.o.f case and will determine which is more efficient. We will also continue the analytical work including extensions to 2 d.o.f, development of a spectral theory for the linearized equations and development of a weakly nonlinear theory to investigate coupling of Fourier modes within and between the σ and π equations. We investigate long term tracking with the averaged equations which should give a speed up of $O(1/\xi)$.

Work supported by DOE contract DE-FG03-99ER41104. Discussions with R. L. Warnock are gratefully acknowledged.

4 REFERENCES

[1] A. W. Chao and R. D. Ruth, *Part.Acc.* **16**, pp. 201–216 (1985)

[2] R. L. Warnock and J. A. Ellison, *Proc.: 2-nd ICFA WS. on High Brightness Beams, UCLA*, Ed.: J. Rosenzweig and L. Serafini, World Scientific, (2000); and *Proc.: 2-nd ICFA Workshop on Quantum Aspects of Beam Phsyics*, Capri, Oct. 2000, to be published by World Scientific.

[3] M. Vogt, T. Sen, J. A. Ellison, FNAL Pub-01/096-T, submitted to Phys. Rev. S.T.–AB (2001)

[4] K. Yokoya and H. Koiso, *Part.Acc.* **27**, pp. 181–186 (1990)

[5] M.–P. Zorzano and F. Zimmermann, *LHC Project Report* **314**, CERN/SL (1999)

[6] L. Greengard, *Thesis*, The MIT PRess Cambridge MA London England (1988); F. W. Jones, *Proc.: Workshop on Space Charge Physics in High Intensity Hadron Rings*, Ed.: A. U. Luccio and W. T. Weng, AIP Conf. Proc. **448**, (1998); W. Herr, M.–P. Zorzano and F. W. Jones, Phys. Rev. S.T.–AB **4** 054402 (2001)